Probing Electric-Dipole-Enabled Transitions in the Excited State of the Nitrogen-Vacancy Center in Diamond

Tom Delord,[1,*] Richard Monge,[1,*] Gabriel I. López-Morales,[1,2] Olaf Bach,[1]
Cyrus E. Dreyer,[3,2] Johannes Flick,[1,4,3] and Carlos A. Meriles[1,4,†]
[1]Department of Physics, CUNY-City College of New York, New York, New York 10031, USA
[2]Department of Physics and Astronomy, Stony Brook University, Stony Brook, New York 11794-3800, USA
[3]Center for Computational Quantum Physics, Flatiron Institute, New York, New York 10010, USA
[4]CUNY-Graduate Center, New York, New York 10016, USA

(Received 28 May 2024; accepted 6 November 2025; published 25 November 2025)

The excited orbitals of color centers often show strong electric dipoles, which can serve as a resource for entanglement, emission tuning, or electric field sensing. Here, we use resonant laser excitation to examine the electric transitions in the excited state (ES) orbitals of the negatively charged nitrogen vacancy center in diamond. By applying microwave electric fields, we perform Rabi driving between ES orbitals, and show that the dressed states can be tuned in frequency and are protected against fluctuations of the transverse electric field. In contrast with previous results, we observe sharp microwave resonances between magnetic states of the ES orbitals, and find that they are broadened due to simultaneous electric dipole driving.

DOI: 10.1103/hp9c-rh23

Color centers in semiconductors and their electron and nuclear spins are widely used quantum sensors [1] and have attractive low temperature properties for quantum computing [2], but the short range of their magnetic interaction [3] means scalable entanglement between centers needs to be mediated, e.g., by photons [4,5]. In that context, larger electric dipoles in the excited states [6,7] (ES) can be used as an alternative resource for entanglement, resonance tuning [8], or electric sensing [9,10]. The high sensitivity of the ES energies to the solid-state environment, however, also creates challenges in the form of spectral diffusion [6,9–11], screening of low frequency electric fields [12,13], and local heterogeneities [14,15].

Here, we use photoluminescence excitation (PLE) spectroscopy to study the impact of microwave (mw) electric fields on the excited orbitals of the negatively charged nitrogen-vacancy (NV) center. We first uncover a previously unobserved electric transition between the two nonmagnetic excited states. PLE spectra reveal the complex features of the dressed state, with the excited state orbitals interacting with the mw electric field via both their longitudinal and transverse dipole moments. For NVs with moderate strain (in the GHz range), resonant mw fields drive Rabi oscillations in the ultrastrong regime without the need for a resonator. The Rabi splitting we obtain allows us to tune the optical resonances by up to ∼0.8 GHz, while creating new eigenstates protected against the electric noise in the NV transverse plane, effectively reducing the inhomogeneous linewidth by a factor of 1.6. We show that under off resonance mw excitation, the PLE resonances become flanked by multiple sidebands, their amplitude governed by an interplay between the Stark effect and the driving of the dipole transition. In contrast with previous results, we lastly observe narrow magnetic resonances in the NV excited states [16–18] and determine that electric driving can broaden them by creating multiple peaks in the energy spectrum. Interestingly, these electric transitions are predictable from theory considerations [19] but have been neither observed nor exploited. While similar physics is obtained using ultrafast optical pulses [20] or acoustic [21] and mechanical [22] resonators, electric transitions hold critical advantages: they can be applied through a standard mw antenna, are readily tuned on and off resonance, and allow for the generation of complex pulse trains with well-defined phase. The fast control of the NV ES orbitals that we demonstrate could be applied to create electric entanglement between proximal NVs or to study other electric-active defects, the NV^0 center in diamond being a recent example [23].

Our experiments take place at 7 K within a closed cycle cryostat, using a homemade confocal microscope to isolate single NVs a few microns deep in a 1-ppb-nitrogen bulk diamond [9,15]. Importantly, both electric and magnetic mw fields stem from a nonoptimized antenna in the form of a 25 μm wire laid on the diamond surface. Figure 1(a) shows a standard PLE spectrum and the measurement sequence we used. A 1 μs green laser pulse initializes the NV into its negative charge (and $|m_S = 0\rangle$ spin) state before we read the photoluminescence (PL) under excitation by a narrow-band tunable laser resonant with the zero-phonon

*These authors contributed equally to this work.
†Contact author: cmeriles@ccny.cuny.edu

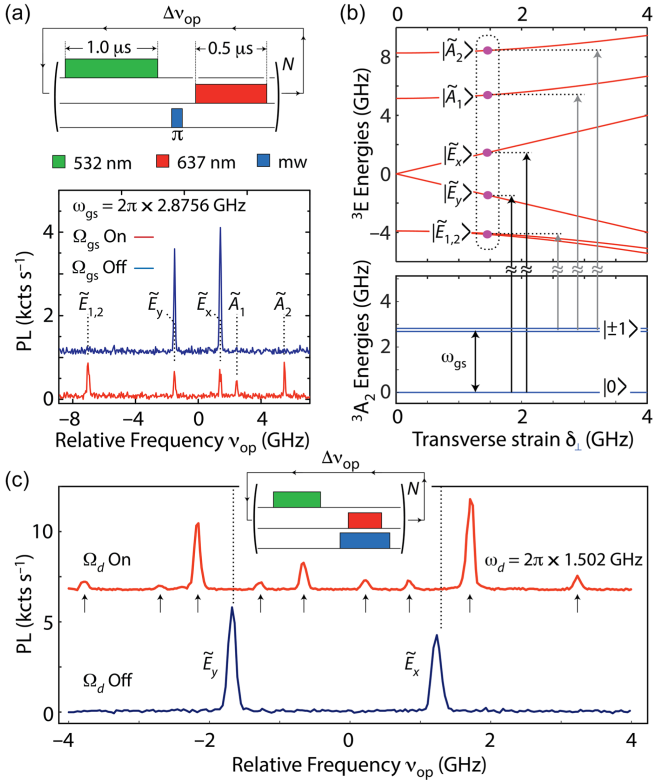

FIG. 1. Optical spectroscopy in the presence of a mw drive. (a) PLE spectroscopy of an individual NV center with ground state initialization into $|0\rangle$ or $|\pm 1\rangle$ (red and blue traces, respectively). The inversion mw pulse is resonant with the ground state zero field splitting, i.e., $\omega_d = \omega_{\mathrm{GS}}$. Here, $N = 10^5$ and $\Delta\nu_{\mathrm{op}} = 53$ MHz. (b) Excited state ^3E and ground state $^3A_2$ energy diagrams (top and bottom, respectively) as a function of transverse strain. Arrows indicate allowed optical transitions from $|0\rangle$ or $|\pm 1\rangle$ (black and gray, respectively). Circles denote the measured excited state energies for the NV in (a). (c) Example PLE spectra ($N = 4 \times 10^5$, $\Delta\nu_{\mathrm{op}} = 27$ MHz) with and without mw drive at $\omega_d = 2\pi \times 1.502$ GHz (red and blue traces, respectively). The presence of mw leads to new optical resonances (arrows). In (a) and (c), green (532 nm) and red (637 nm) blocks denote laser excitation with duration of 1 and 0.5 μs and power of 1.6 mW and 100 nW, respectively; blue squares denote mw excitation at frequency ω_d. In all experiments, the temperature is 7 K; unless indicated, the laser reference frequency is 470.465 THz.

line. Preceding the readout with a mw pulse resonant with the ground state crystal field splitting ω_{GS} allows us to observe the spin dependence of the spectrum. PLE peaks appear when the frequency of the red laser matches one of the six allowed transitions, as depicted in Fig. 1(b). Owing to the p-like character of the ES orbitals, their energies depend on local strain: in particular, the energies of the nonmagnetic orbitals $|E_x\rangle$ and $|E_y\rangle$ split (shift) by an energy proportional to the transverse (longitudinal) strain, leading to states $|\tilde{E}_x\rangle$ and $|\tilde{E}_y\rangle$ in the strained crystal.

Figure 1(c) shows a less conventional PLE measurement for the case of an NV with moderate transverse strain, $\delta_\perp = 2.9$ GHz, where a mw drive runs continuously during optical illumination and PL readout. In this instance, the drive frequency, $\omega_d = 2\pi \times 1.5$ GHz, is far from the ground state magnetic resonance, and we center the PLE spectrum around the $|0\rangle \leftrightarrow |\tilde{E}_x\rangle$ and $|0\rangle \leftrightarrow |\tilde{E}_y\rangle$ lines. Surprisingly, the mw drive has a dramatic impact, shifting the main resonances and creating numerous side peaks at multiples of the drive frequency. We show below that these complex features stem from the combined effects of the longitudinal and transverse electric dipole moments of the NV.

First, the displacement of the main resonance peaks away from each other hints at a coupling term shifting the energies of the mw-dressed states. We confirm this hypothesis by setting the mw tone on resonance with the $|\tilde{E}_x\rangle \leftrightarrow |\tilde{E}_y\rangle$ transition: Fig. 2(a) displays PLE spectra for increasing mw power and shows for both peaks the emergence of Autler-Townes (or Rabi) splitting proportional to the amplitude of the mw drive. Indeed, in the interaction picture with $\mathscr{H}_0 = \omega_d/2(|\tilde{E}_x\rangle\langle\tilde{E}_x| - |\tilde{E}_y\rangle\langle\tilde{E}_y|)$, a coupling term $\mathscr{H}_d = \Omega_d(|\tilde{E}_x\rangle\langle\tilde{E}_y| + |\tilde{E}_y\rangle\langle\tilde{E}_x|)\sin(\omega_d t)$ leads to new eigenstates $|\pm\rangle$ in the $|\tilde{E}_x\rangle$, $|\tilde{E}_y\rangle$ basis subspace with eigenenergies $\omega_\pm = \pm 1/2\sqrt{\Omega_d^2 + \Delta^2}$, where $\Delta = \omega_d - (\omega_x - \omega_y)$ is the drive detuning. Note that the presence of the two pairs of resonances at $\omega_\pm^x$ and $\omega_{\pm/}^y$ straightforwardly arises upon introducing the laser field $H_L = (\Omega_y|0\rangle\langle\tilde{E}_y| + \Omega_x|0\rangle\langle\tilde{E}_x|)e^{\omega_L t} + \mathrm{H.c.}$ and transforming the resulting Hamiltonian to the interaction picture as shown in the Supplemental Material [24].

Interestingly, we find that the $\tilde{E}_x$ and $\tilde{E}_y$ optical resonances are systematically sharper under a resonant mw drive. In Fig. 2(c), we confirm this effect by lowering the laser power well below saturation to observe the inhomogeneous linewidth (broadened by spectral diffusion) [24]. This linewidth then decreases from 98 to 62 MHz, an improvement by a factor of 1.6; a similar effect has been proposed [22] and recently realized with an acoustic drive of the ES orbitals [21]; it ensues from a protection of the dressed states against electric fluctuations in the NV transverse plane. Specifically, if ω_x and ω_y denote the average frequencies of the optical resonances, a small perturbation of the transverse electric field $\epsilon_\perp$ shifts these values to $\omega_x + \epsilon_\perp$ and $\omega_y - \epsilon_\perp$. However, under a drive set at $\omega_d = \omega_x - \omega_y$ we find that a detuning $\Delta = -2\epsilon_\perp$ on the eigenenergies of the modified dressed states $|\pm\rangle$ only shifts the optical resonances by $\pm\epsilon_\perp^2/\Omega_d$ (to first order in $\epsilon_\perp/\Omega_d$) [24]. Intuitively, we see that for a strong enough drive, the two pairs of resonances remain separated by the drive frequency, while without a drive the separation between the $\tilde{E}_x$ and $\tilde{E}_y$ resonances fluctuates with the transverse electric field. The remaining broadening originates from slow fluctuations of the longitudinal electric

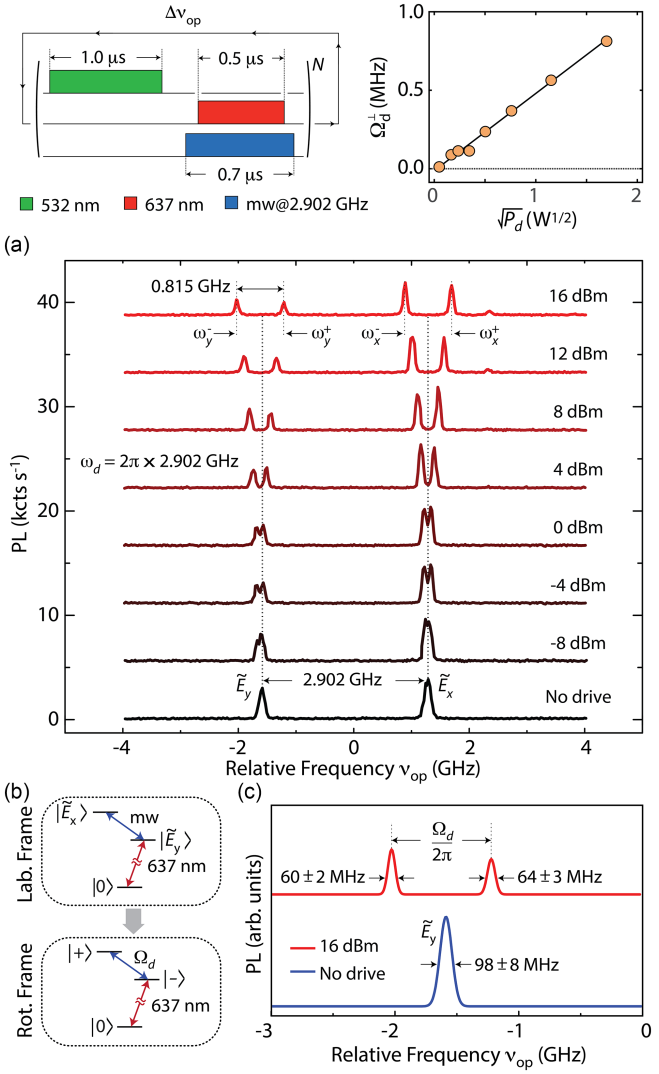

FIG. 2. Dressed states in the ^{3}E manifold. (a) Main: PLE spectroscopy of a single NV under mw excitation resonant with the $|\tilde{E}_x\rangle \leftrightarrow |\tilde{E}_y\rangle$ transition for variable mw power. Upper left: schematics of the pulse sequence. Upper right: Rabi splitting vs the square root of the mw power as derived from the main plot. (b) In the rotating frame description, the $|\tilde{E}_x\rangle$ and $|\tilde{E}_y\rangle$ states hybridize to yield states $|\pm\rangle$ split by the mw Rabi field Ω_d. (c) Enlarged view of the $\tilde{E}_y$ optical resonance with and without mw; Rabi-split peaks show narrower linewidths.

field [9], which could be suppressed by active stabilization, e.g., via an external electric field [36,37], or by adjusting the amplitude of the driving field.

The coupling term $\mathscr{H}_d$ arises from an electric dipole moment $\vec{d}_\perp^{\,es}$, with $\Omega_d = \vec{d}_\perp^{\,es} \cdot \vec{\varepsilon}$ where $\vec{\varepsilon}$ is the electric component of the mw field [24]. Its strength can be experimentally estimated by comparing the Rabi splitting in the optical resonances with the Rabi frequency between the $|0\rangle$ or $|+1\rangle$ states of the ground state manifold $^3A_2$: At the same power and similar frequencies, the Rabi frequency is (50 ± 10) times faster in the excited state. By combining these findings with simulations of our antenna and the experimental determination of the optical dipole orientations [24], we can estimate the mw electric field, and find an electric dipole $(d_\perp^{es})_{exp} = 1.6 \pm 0.4$ D.

To support these findings, we perform first principles calculations. Unlike prior work [19,38,39], our methodology is based on a quantum embedding approach, which treats the NV^- center on a many-body footing, and hence includes important (otherwise missing) electron correlations necessary to attain the highest accuracy [40–42]. Our quantum embedding model yields an amplitude $(d_\perp^{es})_{QE} = 2.16$ D in a direction perpendicular to the plane containing the NV symmetry axis and the strain vector, consistent with the results of a group theoretic description [24,38]. This value is in agreement with the experimental estimate above, and is close to a similar measurement in the NV^0 state [23]. We also calculate the electric dipole along the NV symmetry axis, and find a value $(d_{||}^{es})_{QE} = 1.63$ D, consistent with preceding experimental work [6,10,43].

Since, in general, the electric field we apply has a nonzero component along the NV axis, we can extend our approach to also examine $d_{||}^{es}$ through the use of mw. To this end, we first note that while quasistatic electric fields induce shifts in the optical resonances [6,11–13,44], a periodic drive whose frequency exceeds the inverse excited state lifetime such as ours at ω_d—instead leads to a series of sidebands at multiples of ω_d. Known as Landau-Zener-Stückelberg (LZS) interference fringes [45,46], the amplitude of the nth sideband is typically proportional to $J_n(A/\omega_d)$, where J_n is the Bessel function of the nth kind and A is the drive amplitude [24]. For a weak or moderate drive as in Figs. 3(a) and 3(d), the sideband amplitudes quickly decay with increasing order. In Fig. 3(a), we measure the optical spectrum as a function of the mw frequency for a weak drive amplitude, and observe that only the first two sidebands flanking the $\tilde{E}_y$ transition are above noise, with their amplitude following the variation of the drive due to the frequency-dependent input impedance of the mw circuit.

The system response is expected to change at higher amplitudes because a large enough drive should lead to a frequency comb with the main peak losing intensity. We investigate this limit in Figs. 3(b)–3(d) for a fixed drive frequency $\omega_d = 470$ MHz; this value represents a trade-off as we try to simultaneously make ω_d greater than the inverse excited state lifetime, but sufficiently removed from the $|\tilde{E}_x\rangle \leftrightarrow |\tilde{E}_y\rangle$ transition frequency. Figure 3(d) shows the results: as the mw power increases, we first observe low-order sidebands arising more quickly around the $\tilde{E}_x$ line simply due to a stronger projection of the mw electric field on the $\tilde{E}_x$ than on the $\tilde{E}_y$ dipole. At higher powers a frequency comb arises as predicted, but the sideband pattern is more complex than anticipated, namely, we find that (i) the central peaks corresponding to both $\tilde{E}_x$ and $\tilde{E}_y$

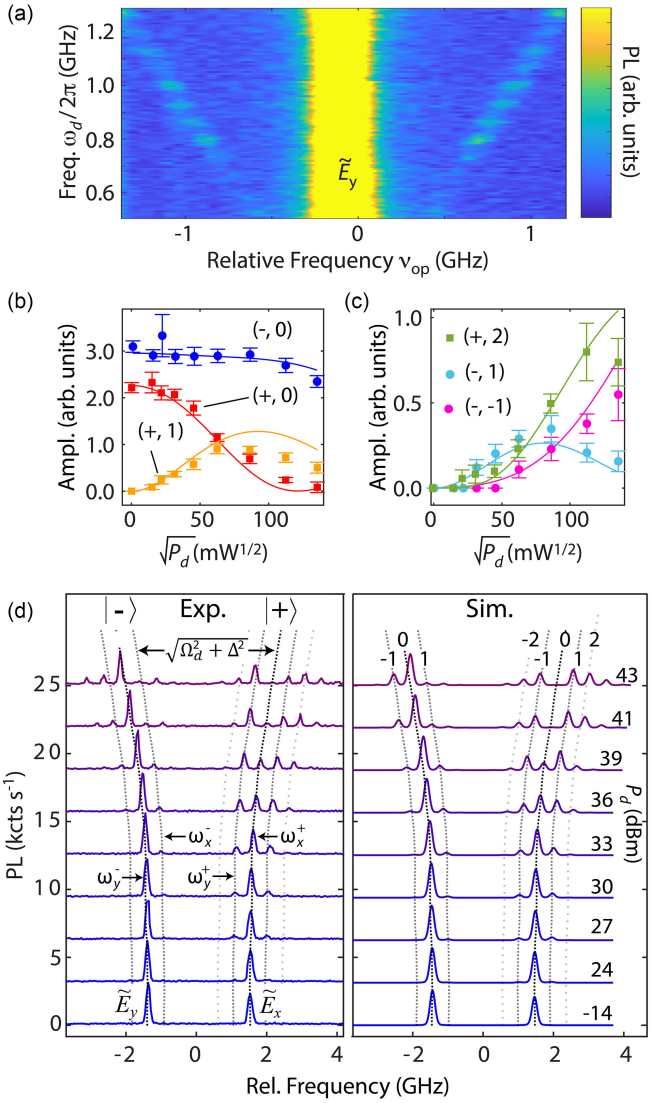

FIG. 3. ac Stark modulation of the NV optical transitions. (a) PLE spectrum near the $\tilde{E}_y$ transition in the presence of mw of variable frequency. The reference frequency is 470.4633 THz. (b),(c) Measured amplitudes of the central PLE resonance as well as four satellites as a function of $\sqrt{P_d}$. Solid lines show fits to the model. The peaks are labeled $(\pm, n)$ with n denoting the sideband order as indicated in (d) compared to the central peak at ω_y^- and ω_x^+. (d) PLE spectroscopy (left) and simulations (right) in the presence of an ac electric field of variable power $P_d \propto |\boldsymbol{A}|^2$ and angular frequency $\omega_d = 2\pi \times 470$ MHz. As P_d increases, dressed states become relevant, and the main resonances show satellites separated from the center frequency by ω_d. Spectra have been shifted vertically for clarity.

lines move away from each other, and (ii) the sideband amplitudes are asymmetric, contrary to what we would expect from the Bessel function symmetry. We attribute both effects to the off resonance excitation of the $|\tilde{E}_x\rangle \leftrightarrow |\tilde{E}_y\rangle$ transition: at higher powers, the Rabi frequency Ω_d becomes comparable to the detuning $\Delta = \omega_d - (\omega_x - \omega_y) \cong -2.4$ GHz, and optical resonances must consider the dressed states $|\pm\rangle$ rather than the bare states $|\tilde{E}_x\rangle$, $|\tilde{E}_y\rangle$. Similar to Fig. 2 and as labeled for the $P_d = 30$–33 dBm curves, this results in two pairs of resonances at $\omega_x^{\pm}$ and $\omega_y^{\pm}$ with an in-pair separation equal to the generalized Rabi frequency and an out-of-pair separation equal to ω_d. The sidebands generated by the Stark effect then overlap within each pair, explaining the asymmetric distribution of their amplitude. To simulate these spectra, we calculate the steady state population in the excited states, using a Lindblad master equation to describe spontaneous emission in the presence of simultaneous laser and mw excitation. The right section of Fig. 3(d) shows the resulting spectra while Figs. 3(b) and 3(c) show the calculated amplitudes of six chosen peaks as a function of the mw amplitude, in all cases yielding good agreement with experiment.

We now turn to transitions between the nonmagnetic and magnetic states in the ^3E manifold. Electron spin resonances (ESR) in the excited states can be observed at room temperature at 1.4 GHz due to orbital averaging [16,18], but have remained elusive at low temperatures [17]. Figures 4(a) and 4(b) show continuous optically detected magnetic resonance spectra (ODMR) under green illumination (1.8 mW, above saturation) for varying mw drive power. While the regular ground state $|0\rangle \leftrightarrow |\pm 1\rangle$ transition is visible at 2.88 GHz, additional features appear close to the energy difference between excited states for the present strain. On the right side [Fig. 4(b)], we observe peaks matching the $|\tilde{E}_x\rangle \leftrightarrow |\tilde{A}_1\rangle$ transition, while on the left side only a low power measurement yields a peak close to the $|\tilde{E}_y\rangle \leftrightarrow |\tilde{E}_{1,2}\rangle$ transitions. In both cases, we find Lorentzian linewidths of about 58 MHz and note the absence of the ^{14}N 40 MHz ES hyperfine splitting [16,47,48], which could be due to a hyperpolarization mechanism or to orbital mixing in the absence of external magnetic fields. At higher power, the $|\tilde{E}_y\rangle \leftrightarrow |\tilde{E}_{1,2}\rangle$ transitions split and broaden into multiple replicas, a feature that we now show is caused by the electric component of the mw drive.

Indeed, at frequencies close to the $|\tilde{E}_x\rangle \leftrightarrow |\tilde{E}_y\rangle$ transition (2.9 GHz), one must consider the dressed states rather than the bare $|\tilde{E}_y\rangle$ orbital. Figure 4(c) shows the evolution of simulated ODMR spectra with power, considering both the $|\tilde{E}_y\rangle \leftrightarrow |\tilde{E}_1\rangle$ transition and the $|\tilde{E}_x\rangle \leftrightarrow |\tilde{E}_y\rangle$ electric transition [24]. Two resonances appear due to the power-dependent Rabi splitting, with the upper transition weaker due to its $|\tilde{E}_x\rangle$ character. Crucially, this implies that the resonant frequencies depend on the mw drive power. Since the amplitude response of our mw antenna is not flat, the same magnetic resonance amplitude can then be found at different frequencies. Figure 4(d) shows how this affects the ODMR spectra by incorporating the frequency response of our mw circuit as measured at the antenna input [24]. Features from the experimental data (shift, broadening,

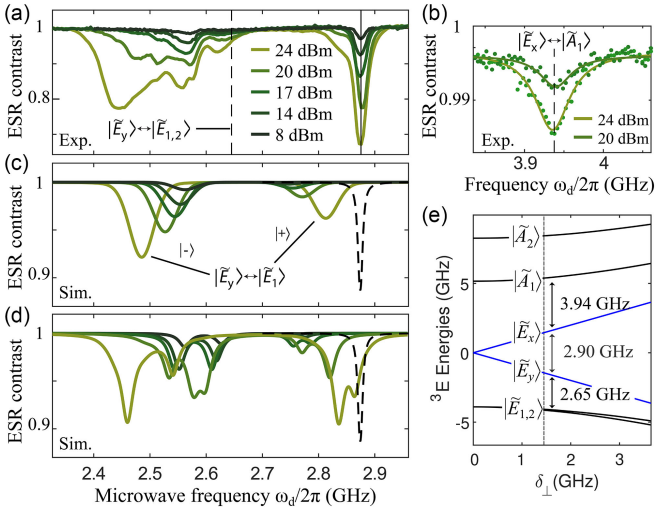

FIG. 4. Optically detected mw resonances under green excitation. (a),(b) Spectra at different mw powers; in (b) solid lines are Gaussian fits yielding a 58 MHz linewidth. Dashed (solid) lines are the expected position for the resonances in the excited (ground) states. Simulated ODMR spectra (c) for a single transition, considering the electric drive that splits the line in two and (d) considering the two lower transitions and accounting for mw power inhomogeneities. The dashed curve is the common $|0\rangle \leftrightarrow |\pm 1\rangle$ ESR dip in the $^3A_2$ manifold. (e) Energy diagram and transition energies as measured from the PLE spectra.

resonance replica) are reproduced reasonably well, though a quantitative match cannot be attained given our inability to measure the exact current at the antenna.

In conclusion, we studied the impact of mw electromagnetic fields on the short-lived NV^- excited states using resonant optical excitation. With a simple wire antenna, we drove strong Rabi oscillations and created LZS interference fringes in the optical spectrum, which we reproduced quantitatively with the help of an analytical model. We found that dressed states are protected against fluctuations of the transverse electric field and allow tuning of the optical resonances [49] without the use of a dc electric field. Combined with our *ab initio* modeling using quantum embedding, our results portend alternative schemes to precision electrometry at the nanoscale, simpler practical approaches to coherently manipulating color centers featuring electric dipoles, and, with them, novel strategies to engineering multiqubit entanglement.

Acknowledgments—The authors acknowledge helpful discussions with Mikhail Lukin. T. D. acknowledges support by the U.S. Department of Energy, Office of Science, National Quantum Information Science Research Centers, Co-design Center for Quantum Advantage (C2QA) under Contract No. DE-SC0012704. R. M. and C. A. M. acknowledge support from the National Science Foundation through Grants No. NSF-2514938, No. NSF-2506082, and No. NSF-2203904. R. M. also acknowledges support from NSF-2316693. J. F. acknowledges support from NSF Grant No. NSF-2216838. G. I. L. M. acknowledges grant NSF-2208863. C. E. D acknowledges support from NSF Grant No. DMR-2237674. All authors acknowledge access to the facilities and research infrastructure of the NSF CREST IDEALS, Grant No. NSF-2112550. The Flatiron Institute is a division of the Simons Foundation.

Data availability—The data that support the findings of this article are not publicly available upon publication because it is not technically feasible and/or the cost of preparing, depositing, and hosting the data would be prohibitive within the terms of this research project. The data are available from the authors upon reasonable request.

[1] C. L. Degen, F. Reinhard, and P. Cappellaro, Quantum sensing, Rev. Mod. Phys. **89**, 035002 (2017).
[2] C. Bradac, W. Gao, J. Forneris, M. E. Trusheim, and I. Aharonovich, Quantum nanophotonics with group IV defects in diamond, Nat. Commun. **10**, 5625 (2019).
[3] F. Dolde, I. Jakobi, B. Naydenov, N. Zhao, S. Pezzagna, C. Trautmann, J. Meijer, P. Neumann, F. Jelezko, and J. Wrachtrup, Room-temperature entanglement between single defect spins in diamond, Nat. Phys. **9**, 139 (2013).
[4] H. Bernien, B. Hensen, W. Pfaff, G. Koolstra, M. S. Blok, L. Robledo, T. H. Taminiau, M. Markham, D. J. Twitchen, L. Childress, and R. Hanson, Heralded entanglement between solid-state qubits separated by three metres, Nature (London) **497**, 86 (2013).
[5] R. E. Evans, M. K. Bhaskar, D. D. Sukachev, C. T. Nguyen, A. Sipahigil, M. J. Burek, B. Machielse, G. H. Zhang, A. S. Zibrov, E. Bielejec, H. Park, M. Loncar, and M. D. Lukin, Photon-mediated interactions between quantum emitters in a diamond nanocavity, Science **362**, 662 (2018).
[6] Ph. Tamarat, T. Gaebel, J. R. Rabeau, M. Khan, A. D. Greentree, H. Wilson, L. C. L. Hollenberg, S. Prawer, P. Hemmer, F. Jelezko, and J. Wrachtrup, Stark shift control of single optical centers in diamond, Phys. Rev. Lett. **97**, 083002 (2006).
[7] C. P. Anderson, A. Bourassa, K. C. Miao, G. Wolfowicz, P. J. Mintun, A. L. Crook, H. Abe, J. Ul-Hassan, N. T. Son, T. Ohshima, and D. D. Awschalom, Electrical and optical control of single spins integrated in scalable semiconductor devices, Science **366**, 1225 (2019).
[8] H. Bernien, L. Childress, L. Robledo, M. Markham, D. Twitchen, and R. Hanson, Two-photon quantum interference from separate nitrogen vacancy centers in diamond, Phys. Rev. Lett. **108**, 043604 (2012).
[9] T. Delord, R. Monge, and C. A. Meriles, Correlated spectroscopy of electric noise with color center clusters, Nano Lett. **24**, 6474 (2024).
[10] W. Ji, Z. Liu, Y. Guo, Z. Hu, J. Zhou, S. Dai, Y. Chen, P. Yu, M. Wang, K. Xia, F. Shi, Y. Wang, and J. Du, Correlated sensing with a solid-state quantum multisensor system for atomic-scale structural analysis, Nat. Photonics **18**, 230 (2024).
[11] B. A. McCullian, H. F. H. Cheung, H. Y. Chen, and G. D. Fuchs, Quantifying the spectral diffusion of N-V centers by symmetry, Phys. Rev. Appl. **18**, 064011 (2022).

[12] L. C. Bassett, F. J. Heremans, C. G. Yale, B. B. Buckley, and D. D. Awschalom, Electrical tuning of single nitrogen-vacancy center optical transitions enhanced by photoinduced fields, Phys. Rev. Lett. **107**, 266403 (2011).
[13] V. M. Acosta, C. Santori, A. Faraon, Z. Huang, K.-M. C. Fu, A. Stacey, D. A. Simpson, K. Ganesan, S. Tomljenovic-Hanic, A. D. Greentree, S. Prawer, and R. G. Beausoleil, Dynamic stabilization of the optical resonances of single nitrogen-vacancy centers in diamond, Phys. Rev. Lett. **108**, 206401 (2012).
[14] A. Sipahigil, K. D. Jahnke, L. J. Rogers, T. Teraji, J. Isoya, A. S. Zibrov, F. Jelezko, and M. D. Lukin, Indistinguishable photons from separated silicon-vacancy centers in diamond, Phys. Rev. Lett. **113**, 113602 (2014).
[15] R. Monge, T. Delord, and C. A. Meriles, Reversible optical data storage below the diffraction limit, Nat. Nanotechnol. **19**, 202 (2024).
[16] G. D. Fuchs, V. V. Dobrovitski, R. Hanson, A. Batra, C. D. Weis, T. Schenkel, and D. D. Awschalom, Excited-state spectroscopy using single spin manipulation in diamond, Phys. Rev. Lett. **101**, 117601 (2008).
[17] A. Batalov, V. Jacques, F. Kaiser, P. Siyushev, P. Neumann, L. J. Rogers, R. L. McMurtrie, N. B. Manson, F. Jelezko, and J. Wrachtrup, Low temperature studies of the excited-state structure of negatively charged nitrogen-vacancy color centers in diamond, Phys. Rev. Lett. **102**, 195506 (2009).
[18] P. Neumann, R. Kolesov, V. Jacques, J. Beck, J. Tisler, A. Batalov, L. Rogers, N. B. Manson, G. Balasubramanian, F. Jelezko, and J. Wrachtrup, Excited-state spectroscopy of single NV defects in diamond using optically detected magnetic resonance, New J. Phys. **11**, 013017 (2009).
[19] J. R. Maze, A. Gali, E. Togan, Y. Chu, A. Trifonov, E. Kaxiras, and M. D. Lukin, Properties of nitrogen-vacancy centers in diamond: The group theoretic approach, New J. Phys. **13**, 025025 (2011).
[20] L. C. Bassett, F. J. Heremans, D. J. Christle, C. G. Yale, G. Burkard, B. B. Buckley, and D. D. Awschalom, Ultrafast optical control of orbital and spin dynamics in a solid-state defect, Science **345**, 1333 (2014).
[21] B. A. McCullian, V. Sharma, H. Y. Chen, J. C. Crossman, E. J. Mueller, and G. D. Fuchs, Coherent acoustic control of defect orbital states in the strong-driving limit, PRX Quantum **5**, 030336 (2024).
[22] H. Y. Chen, E. R. MacQuarrie, and G. D. Fuchs, Orbital state manipulation of a diamond nitrogen-vacancy center using a mechanical resonator, Phys. Rev. Lett. **120**, 167401 (2018).
[23] H. Kurokawa, K. Wakamatsu, S. Nakazato, T. Makino, H. Kato, Y. Sekiguchi, and H. Kosaka, Coherent electric field control of orbital state of a neutral nitrogen-vacancy center, Nat. Commun. **15**, 4039 (2024).
[24] See Supplemental Material at http://link.aps.org/supplemental/10.1103/hp9c-rh23, which also contains Refs. [25–35].
[25] M. W. Doherty, N. B. Manson, P. Delaney, F. Jelezko, J. Wrachtrup, and L. C. L. Hollenberg, The nitrogen-vacancy colour centre in diamond, Phys. Rep. **528**, 1 (2013).
[26] S. Ashhab, J. R. Johansson, A. M. Zagoskin, and F. Nori, Two-level systems driven by large-amplitude fields, Phys. Rev. A **75**, 063414 (2007).
[27] L. J. Rogers, R. L. McMurtrie, M. J. Sellars, and N. B. Manson, Time-averaging within the excited state of the nitrogen-vacancy centre in diamond, New J. Phys. **11**, 063007 (2009).
[28] R. Monge, T. Delord, G. Thiering, Á. Gali, and C. A. Meriles, Resonant versus non-resonant spin readout of a nitrogen-vacancy center in diamond under cryogenic conditions, Phys. Rev. Lett. **131**, 236901 (2023).
[29] R. Monge, T. Delord, N. Proscia, Z. Shotan, H. Jayakumar, J. Henshaw, P. Zangara, A. Lozovoi, D. Pagliero, P. D. Esquinazi, T. An, I. Sodemann, V. M. Menon, and C. A. Meriles, Spin dynamics of a solid-state qubit in proximity to a superconductor, Nano Lett. **23**, 422 (2023).
[30] T. Yoon, M. Cha, D. Kim, and H. Choi, Identifying NV center axes via spatially varying microwave fields for vector magnetometry, Appl. Phys. Lett. **126**, 144002 (2025).
[31] K. W. Lee, D. Lee, P. Ovartchaiyapong, J. Minguzzi, J. R. Maze, and A. C. Bleszynski Jayich, Strain coupling of a mechanical resonator to a single quantum emitter in diamond, Phys. Rev. Appl. **6**, 034005 (2016).
[32] P. Wang, Z. Yuan, P. Huang, X. Rong, M. Wang, X. Xu, C. Duan, C. Ju, F. Shi, and J. Du, High-resolution vector microwave magnetometry based on solid-state spins in diamond, Nat. Commun. **6**, 6631 (2015).
[33] G. Kresse and J. Furthmüller, Efficient iterative schemes for *ab initio* total-energy calculations using a plane-wave basis set, Phys. Rev. B **54**, 11169 (1996).
[34] G. Kresse and D. Joubert, From ultrasoft pseudopotentials to the projector augmented-wave method, Phys. Rev. B **59**, 1758 (1999).
[35] J. Heyd, G. E. Scuseria, and M. Ernzerhof, Hybrid functionals based on a screened Coulomb potential, J. Chem. Phys. **118**, 8207 (2003).
[36] V. M. Acosta, C. Santori, A. Faraon, Z. Huang, K.-M. C. Fu, A. Stacey, D. A. Simpson, K. Ganesan, S. Tomljenovic-Hanic, A. D. Greentree, S. Prawer, and R. G. Beausoleil, Dynamic stabilization of the optical resonances of single nitrogen-vacancy centers in diamond, Phys. Rev. Lett. **108**, 206401 (2012).
[37] H. Bernien, L. Childress, L. Robledo, M. Markham, D. Twitchen, and R. Hanson, Two-photon quantum interference from separate nitrogen vacancy centers in diamond, Phys. Rev. Lett. **108**, 043604 (2012).
[38] Á. Gali, *Ab-initio* theory of the nitrogen-vacancy center in diamond, Nanophotonics **8**, 1907 (2019).
[39] L. Alaerts, Y. Xiong, S. Griffin, and G. Hautier, A first principles study of the Stark shift effect on the zero-phonon line of the NV center in diamond, arXiv:2403.07771.
[40] M. Bockstedte, F. Schütz, T. Garratt, V. Ivády, and A. Gali, *Ab initio* description of highly correlated states in defects for realizing quantum bits, npj Quantum Mater. **3**, 1 (2018).
[41] L. Muechler, D. I. Badrtdinov, A. Hampel, J. Cano, M. Rösner, and C. E. Dreyer, Quantum embedding methods for correlated excited states of point defects: Case studies and challenges, Phys. Rev. B **105**, 235104 (2022).
[42] G. I. López-Morales, J. M. Zajac, J. Flick, C. A. Meriles, and C. E. Dreyer, Quantum embedding study of strain and charge induced Stark effects on the NV^- center in diamond, Phys. Rev. B **110**, 245127 (2024).

[43] M. Block, B. Kobrin, A. Jarmola, S. Hsieh, C. Zu, N. L. Figueroa, V. M. Acosta, J. Minguzzi, J. R. Maze, D. Budker, and N. Y. Yao, Optically enhanced electric field sensing using nitrogen-vacancy ensembles, Phys. Rev. Appl. **16**, 024024 (2021).

[44] K.-M. C. Fu, C. Santori, P. E. Barclay, L. J. Rogers, N. B. Manson, and R. G. Beausoleil, Observation of the dynamic Jahn-Teller effect in the excited states of nitrogen-vacancy centers in diamond, Phys. Rev. Lett. **103**, 256404 (2009).

[45] S. N. Shevchenko, S. Ashhab, and F. Nori, Landau–Zener–Stückelberg interferometry, Phys. Rep. **492**, 1 (2010).

[46] K. C. Miao, A. Bourassa, C. P. Anderson, S. J. Whiteley, A. L. Crook, S. L. Bayliss, G. Wolfowicz, G. Thiering, P. Udvarhelyi, V. Ivády, H. Abe, T. Ohshima, Á. Gali, and D. D. Awschalom, Electrically driven optical interferometry with spins in silicon carbide, Sci. Adv. **5**, eaay0527 (2019).

[47] M. Steiner, P. Neumann, J. Beck, F. Jelezko, and J. Wrachtrup, Universal enhancement of the optical readout fidelity of single electron spins at nitrogen-vacancy centers in diamond, Phys. Rev. B **81**, 035205 (2010).

[48] G. D. Fuchs, V. V. Dobrovitski, D. M. Toyli, F. J. Heremans, C. D. Weis, T. Schenkel, and D. D. Awschalom, Excited-state spin coherence of a single nitrogen–vacancy centre in diamond, Nat. Phys. **6**, 668 (2010).

[49] D. M. Lukin, A. D. White, R. Trivedi, M. A. Guidry, N. Morioka, C. Babin, Ö. O. Soykal, J. Ul-Hassan, N. T. Son, T. Ohshima, P. K. Vasireddy, M. H. Nasr, S. Sun, J.-P. W. MacLean, C. Dory, E. A. Nanni, J. Wrachtrup, F. Kaiser, and J. Vučković, Spectrally reconfigurable quantum emitters enabled by optimized fast modulation, npj Quantum Inf. **6**, 80 (2020).